The Astrophysical Journal, 799:39 (8pp), 2015 January 20 doi:10.1088/0004-637X/799/1/39
© 2015. The American Astronomical Society. All rights reserved.

RELATIVISTIC ($E > 0.6$, > 2.0, AND > 4.0 MeV) ELECTRON ACCELERATION AT GEOSYNCHRONOUS ORBIT DURING HIGH-INTENSITY, LONG-DURATION, CONTINUOUS AE ACTIVITY (HILDCAA) EVENTS

Rajkumar Hajra[1], Bruce T. Tsurutani[2], Ezequiel Echer[1], Walter D. Gonzalez[1], and Ondrej Santolik[3,4]
[1] Instituto Nacional de Pesquisas Espaciais (INPE), Av. dos Astronautas, 1758, São José dos Campos, São Paulo 12227-010, Brazil; rajkumarhajra@yahoo.co.in
[2] Jet Propulsion Laboratory, California Institute of Technology, 4800 Oak Grove Drive Pasadena, Pasadena, CA 91109, USA
[3] Institute of Atmospheric Physics AS CR, Prague, Czech Republic
[4] Faculty of Mathematics and Physics, Charles University, Prague, Czech Republic
Received 2014 August 27; accepted 2014 November 5; published 2015 January 14

ABSTRACT

Radiation-belt relativistic ($E > 0.6$, > 2.0, and > 4.0 MeV) electron acceleration is studied for solar cycle 23 (1995–2008). High-intensity, long-duration, continuous AE activity (HILDCAA) events are considered as the basis of the analyses. All of the 35 HILDCAA events under study were found to be characterized by flux enhancements of magnetospheric relativistic electrons of all three energies compared to the pre-event flux levels. For the $E >$ 2.0 MeV electron fluxes, enhancement of >50% occurred during 100% of HILDCAAs. Cluster-4 passes were examined for electromagnetic chorus waves in the $5 < L < 10$ and $0 <$ MLT < 12 region when wave data were available. Fully 100% of these HILDCAA cases were associated with enhanced whistler-mode chorus waves. The enhancements of $E > 0.6$, > 2.0, and > 4.0 MeV electrons occurred ∼1.0 day, ∼1.5 days, and ∼2.5 days after the statistical HILDCAA onset, respectively. The statistical acceleration rates for the three energy ranges were $\sim 1.8 \times 10^5$, 2.2×10^3, and 1.0×10^1 cm^{-2} s^{-1} sr^{-1} d^{-1}, respectively. The relativistic electron-decay timescales were determined to be ∼7.7, 5.5, and 4.0 days for the three energy ranges, respectively. The HILDCAAs were divided into short-duration ($D \leqslant 3$ days) and long-duration ($D > 3$ days) events to study the dependence of relativistic electron variation on HILDCAA duration. For long-duration events, the flux enhancements during HILDCAAs with respect to pre-event fluxes were ∼290%, 520%, and 82% for $E > 0.6$, > 2.0, and > 4.0 MeV electrons, respectively. The enhancements were ∼250%, 400%, and 27% respectively, for short-duration events. The results are discussed with respect to the current understanding of radiation-belt dynamics.

Key words: acceleration of particles – magnetic reconnection – relativistic processes – solar wind – waves

1. INTRODUCTION

The acceleration of relativistic (MeV) electrons within the Earth's outer radiation belt ($L > 3.5$) is both an interesting physical phenomenon (Paulikas & Blake 1979; Baker et al. 1986, 1999) and a hazard to orbiting spacecraft (Wrenn 1995; Horne 2003). Relativistic electrons were initially reported by Paulikas & Blake (1979), who noted that electrons appeared in association with high-speed solar wind streams (HSSs) impinging upon the magnetosphere. One scenario to possibly explain this relationship was given by Tsurutani et al. (2010). The scenario is as follows. The HSSs are accompanied by embedded Alfvén waves generated by supergranule circulation at the Sun. The waves are convected to 1 AU and beyond by the solar wind (Belcher & Davis 1971; Tsurutani et al. 1994). The southward component of the Alfvén waves causes magnetic reconnection at the Earth's dayside magnetopause (Dungey 1961; Gonzalez & Mozer 1974; Tsurutani et al. 1995), leading to substorms and convection events and energetic ∼10–100 keV electron injections into the nightside sector of the magnetosphere (DeForest & McIlwain 1971; Horne & Thorne 1998). The temperature anisotropy of the heated electrons leads to plasma instability (Kennel & Petschek 1966; Tsurutani & Lakhina 1997), generating electromagnetic plasma waves called "chorus" (Tsurutani & Smith 1977; Meredith et al. 2001; Tsurutani et al. 2013). Resonant interactions of the chorus waves with ∼100 keV electrons lead to the acceleration to relativistic energies (Inan et al. 1978; Horne & Thorne 1998; Thorne et al. 2005, 2013; Summers et al. 2007; Reeves et al. 2013; Boyd et al. 2014).

Another consequence of long-duration, sporadic magnetic reconnection by the southward component of the interplanetary Alfvén waves is the occurrence of prolonged periods of moderate-intensity geomagnetic activity (AE) at the Earth. This geomagnetic activity can last for days to weeks (Tsurutani et al. 1995, 2006; Gonzalez et al. 2006; Guarnieri 2006; Kozyra et al. 2006; Turner et al. 2006; Hajra et al. 2013). The geomagnetic activity has been called high-intensity, long-duration, continuous AE activity (HILDCAA) events (Tsurutani & Gonzalez 1987). These events may be particularly effective in the relativistic electron-acceleration process (Hajra et al. 2013). It was shown (Hajra et al. 2014c) that the lengthy and continuous intervals of AE activity are ideal for electron acceleration.

In the present effort, we analyze relativistic electrons at three different energy levels: $E > 0.6$, > 2.0, and > 4.0 MeV at geosynchronous orbit ($L = 6.6$) to investigate the electron flux dependence on HILDCAA temporal length, if there is any. Relativistic electron acceleration and decay timescales will also be studied, which may be important for magnetospheric modeling. The statistical studies will be based on superposed epoch analyses of relativistic electron fluxes along with solar wind/interplanetary and geomagnetic data. HILDCAA events occurring during the entire solar cycle (SC) 23, from 1995 through 2008, are used as a basis for superposed epoch analyses.

2. DATA AND METHOD OF ANALYSES

As mentioned above, HILDCAAs are used as the main basis of the statistical studies and the superposed epoch analyses in this effort. HILDCAAs are distinguished from mechanisms that create geomagnetic storm main phases by four strictly defined

criteria (Tsurutani & Gonzalez 1987). By definition, HILDCAAs are intervals of intense auroral activity characterized by peak AE intensities greater than 1000 nT and a minimum of two days duration where AE values do not drop below 200 nT for more than 2 hr at a time. These events are also defined to occur outside the main phases of geomagnetic storms. From a list of HILDCAA events occurring during ∼3.5 solar cycles (1975–2011) prepared by Hajra et al. (2013), we selected the 35 events that occurred during the most recent (full) solar cycle (SC 23) (Hajra et al. 2014a, 2014c) when solar wind/interplanetary and relativistic electron data are available. To avoid the effects of geomagnetic storms (with Dst $\leqslant -50$ nT; Gonzalez et al. 1994), we selected only events that were not preceded by storms for this study.

Solar wind/interplanetary data at 1 minute time resolution were obtained from the OMNI website (http://omniweb.gsfc.nasa.gov/). OMNI interplanetary data had already been time adjusted to take into account the solar wind convection time from the spacecraft to the bow shock, so no further adjustment to the interplanetary data was made in this study.

The integrated fluxes of electrons with energies $E > 0.6$, > 2.0, and > 4.0 MeV at geosynchronous orbit ($L = 6.6$) are collected from the *Geostationary Operational Environment Satellites* (*GOES*; http://www.ngdc.noaa.gov/stp/satellite/goes/dataaccess.html). For general time coverage, data for events during 1995–2002 are obtained from GOES-8 and those for 2003–2008 events from GOES-12. The satellites carry space environment monitoring instrument subsystems onboard that provide magnetometer, energetic particle, and soft X-ray data. The electron fluxes used in the present study were measured by solid-state detectors with pulse height discrimination in the energetic particle sensors. The data were corrected for secondary responses from other energies (e.g., protons > 32 MeV) and from directions outside the nominal detector entrance apertures. See Onsager et al. (1996) for more details about the *GOES* particle detectors. For the statistical analysis on the relativistic particle fluxes, we used running daily averages of the 1 minute data to remove diurnal variations, which are well-known features of geosynchronous flux data (e.g., Turner & Li 2008).

There was no plasma wave detector onboard either GOES-8 or GOES-12. Thus, to study whether chorus is detected during HILDCAA intervals, wave information was taken from the Cluster-4 satellite (Santolik et al. 2014). Because chorus is generated by clouds of anisotropic energetic ∼10–100 keV electrons (Tsurutani et al. 1979) that have been injected into the magnetosphere in the midnight sector and then gradient drifted through dawn to local noon, there will be multiple clouds of these energetic electrons drifting through the magnetosphere at any time. Thus, chorus would be expected to be present in the midnight-to-dawn sector because of the freshly injected anisotropic electrons (Tsurutani & Smith 1974; Meredith et al. 2001, 2012; Santolik et al. 2009, 2010) and also in the dawn-to-noon local time sector where the energetic electrons could become unstable because of the higher thermal plasma densities at this location (Tsurutani et al. 1977; Meredith et al. 2001, 2012). The high plasma densities in this local time sector have been ascribed to increased solar photoionization and heating of the atmosphere (Brice & Lucas 1971; Jentsch 1976).

It is not certain at what local times the ∼100 keV electrons are accelerated to approximately MeV energies, but one might suspect that it will occur where chorus is most intense, e.g., the local time sector mentioned above. Relativistic electrons gradient drift around the magnetosphere quite rapidly (∼5 minutes), so once they are accelerated, they end up forming an amorphous "belt" in the outer zone of the magnetosphere. Therefore, one cannot expect there to be a one-to-one relationship between chorus and relativistic electrons, and therefore one was not sought.

What one can do, however, is show a consistency of the relationship between HILDCAAs and chorus and chorus and relativistic electrons. In this paper, we will look for Cluster-4 passes between 00 and 6 MLT, 6 and 12 MLT, and $L = 5$–10 to determine how often chorus is present during HILDCAA intervals.

3. RESULTS

3.1. Event Case Study

Figure 1 shows an example of solar/interplanetary variations as well as geomagnetic and radiation belt effects during an HILDCAA event on 2003 September 15–20. As denoted by the horizontal line in the AE panel, the HILDCAA event started at ∼2102 UT on day 258 (September 15) and continued for ∼5 days until ∼2203 UT on day 263 (September 20). The HILDCAA event is associated with a corotating interaction region (CIR), as indicated by the compressed plasma density (Nsw) and interplanetary magnetic field (IMF Bo) during the start of day 259 to the middle of day 260. The CIR is followed by an HSS event. It is interesting to note that the HILDCAA event started with the CIR that did not cause a geomagnetic storm for this case—the peak Dst during the CIR event was only −48 nT. The HSS interval is characterized by long-term moderate geomagnetic activity with peak Dst of −57 nT and peak AE of 2072 nT. The onset of the HILDCAA event coincides with a north-to-southward turning of the IMF Bz component, which is established to be the general statistical feature of HILDCAAs (Hajra et al. 2013, 2014b). The same period is also associated with negative and positive polarity reversals of the B_x and B_y components of the IMF, respectively. The IMF component changes indicate a typical heliospheric current sheet (HCS) crossing (Smith et al. 1978; Tsurutani et al. 1995). The HCS is denoted by a vertical line in the figure and occurs here prior to the stream–stream interaction. The HILDCAA event occurred during the fall equinox and was in a "geoeffective" positive-IMF sector region (see the sector polarity of the solar wind as listed in the Wilcox Solar Observatory: http://wso.standford.edu/).

The top panel of Figure 1 shows the variations of the integrated electron fluxes (in units of $\mathrm{cm^{-2}\ s^{-1}\ sr^{-1}}$, hereafter called flux unit, FU) at two energy levels: $E > 0.6$ and > 2.0 MeV from GOES-8. The HILDCAA initiation is associated with electron flux "dropout" occurring during the CIR event. Interestingly, the electron flux decrease coincides with the HCS crossing during the end of day 258 (September 15). Electron fluxes start to increase around the middle of day 260 (September 17) at the far end of the CIR. The time lags (>1 day and ∼1.5 days) of relativistic electron flux enhancements ($E > 0.6$ and > 2.0 MeV, respectively) from the HILDCAA initiation time are consistent with the statistical result of Hajra et al. (2014c). The entire HILDCAA interval thereafter is associated with enhanced fluxes of relativistic electrons.

An example of whistler-mode chorus wave generation during 1800–2100 UT on 2003 September 16 is shown in Figure 2. The red and yellow traces starting at ∼1830 UT at ∼4 kHz and descending to ∼400 Hz by ∼1945 UT are the chorus waves (marked by a red rectangle). This interval corresponds to $L = 4.6$ to ∼13, the entire outer-zone magnetosphere between the nominal location of the plasmasphere to the magnetopause. The

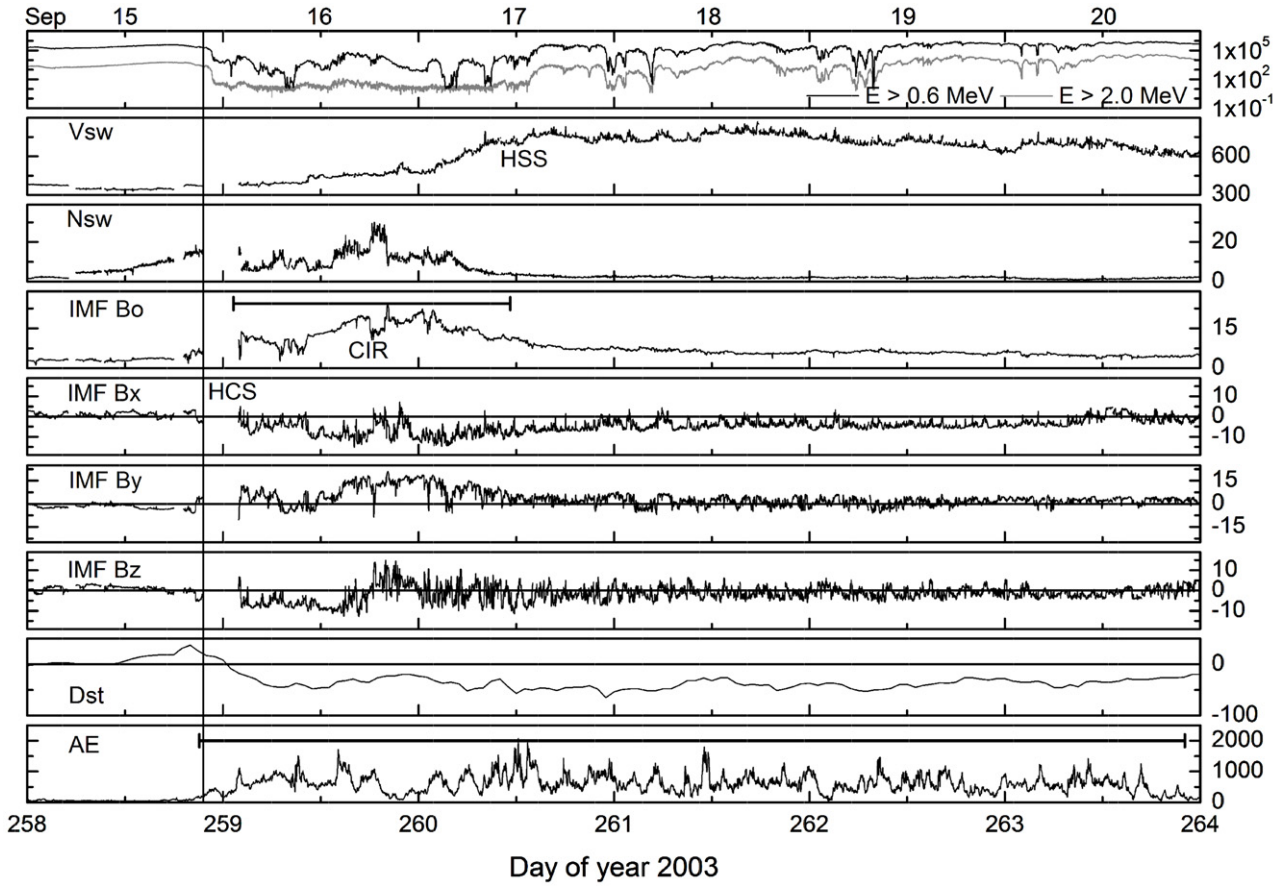

Figure 1. Solar wind/interplanetary dependences and geomagnetic and radiation belt effects during a HILDCAA event occurring on 2003 September 15–20. From top to bottom, the panels show the variations of $E > 0.6$ (black curve) and > 2.0 MeV (gray curve) electron fluxes ($cm^{-2}\ s^{-1}\ sr^{-1}$) from GOES-8, solar wind speed (Vsw in km s^{-1}), plasma density (Nsw in cm^{-3}), IMF magnitude (Bo in nT), and Bx (nT), By (nT), Bz (nT) components in the GSM coordinate system, and the Dst (nT) and AE (nT) indices, respectively. In the AE panel, the horizontal line indicates the time interval of the HILDCAA event. The horizontal line in the IMF Bo panel shows the CIR interval. The HCS is shown by a vertical line.

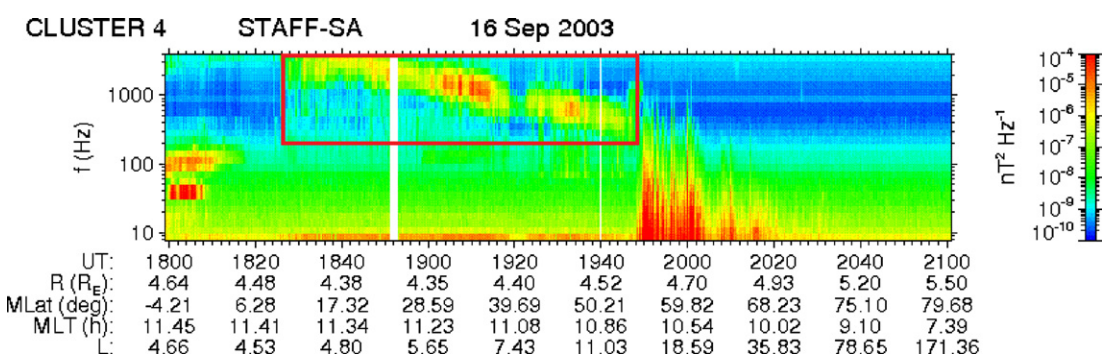

Figure 2. Frequency–time spectrogram of the magnetic field component of chorus measured by the Cluster-4 spacecraft on 2003 September 16 during the 1800–2100 UT period. The red and yellow trace starting at ∼1830 UT at ∼4 kHz and descending to ∼400 Hz by ∼1945 UT are the chorus signals. This region is marked by a red rectangle.

MLT for this interval was 11.4 to 10.5, a region where chorus is particularly intense.

Cluster-4 data is available for 16 HILDCAA events occurring between 2001 and 2008 where Cluster-4 was in the $5 < L < 10$, $00 < \mathrm{MLT} < 6$, and $6 < \mathrm{MLT} < 12$ regions. We find that all of these 16 events were associated with chorus events in both local time sectors. Thus, chorus was detected 100% of the time that Cluster-4 was in a proper location ($00 < \mathrm{MLT} < 12$).

In the following sections, we present statistical studies and superposed epoch analyses on the relativistic electrons as well as solar wind/interplanetary and geomagnetic parameters. The time of HILDCAA initiation (based on the criteria stated in Section 2) is taken as the reference time ($t = 0$) of the superposed analyses.

3.2. Relativistic Electron Flux Response During HILDCAA Events

To quantify the response of relativistic electron fluxes during HILDCAA events, we estimated the peak flux values during 1 day before HILDCAA initiation and during the interval of individual HILDCAA events. We call these "premax" and "postmax" fluxes, respectively. As mentioned in Section 2, the

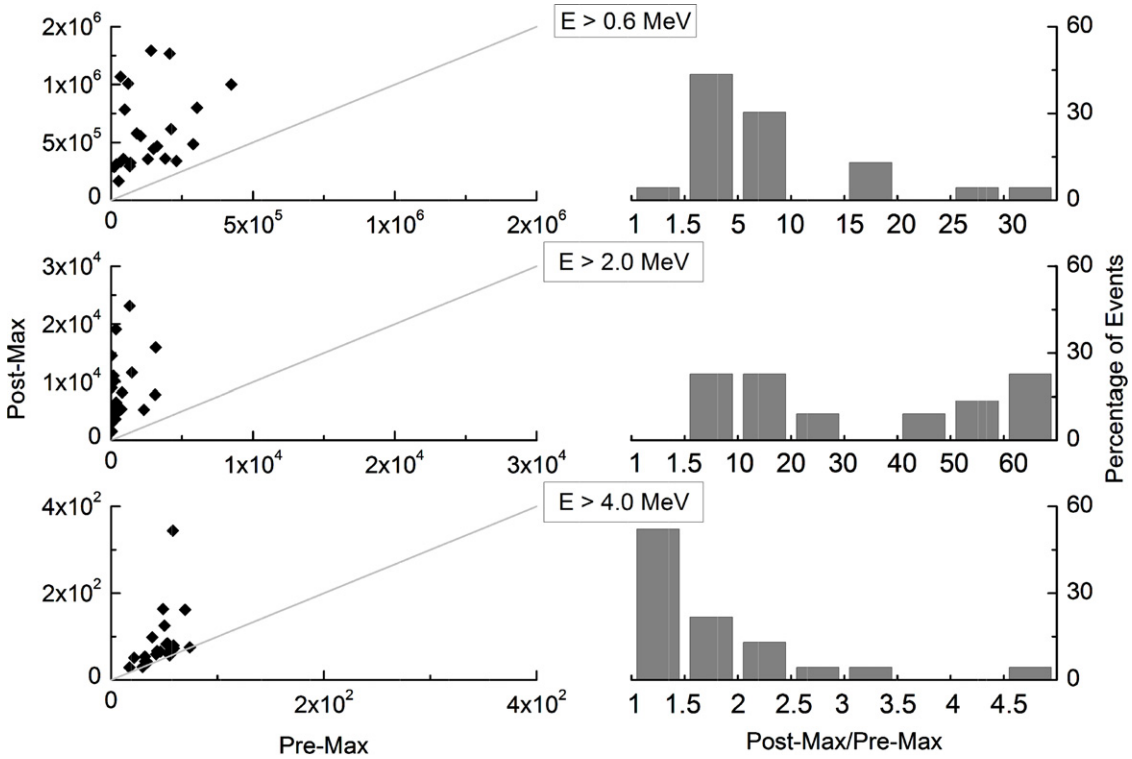

Figure 3. Left panel: variations of peak relativistic electron fluxes (cm^{-2} s^{-1} sr^{-1}) after HILDCAA initiation (postmax) against those before HILDCAA initiation (premax). The gray straight line in each panel shows the postmax = premax line. Right panel: the distributions (%) of the ratio of the postmax to premax fluxes. The energy levels of the electrons are given in each panel.

running daily averages of the fluxes (1 minute time resolution) are used for this study. In the left panel of Figure 3 we plot the postmax fluxes against the premax ones for each HILDCAA event. It is observed that fluxes after the HILDCAA initiation are not correlated with those before the initiation. Another feature to note is that the data points are always above the postmax = premax lines (gray straight lines). This implies that the peak fluxes after HILDCAA initiation are always greater than those before HILDCAA initiation, i.e., HILDCAAs are always associated with flux enhancements of magnetospheric relativistic electrons of all three energies. We arbitrarily define "significant enhancement of flux" if the flux increase is greater than a factor of 1.5 (i.e., >50% increase). The right panel of Figure 3 shows the percentage distribution of HILDCAA events as a function of the ratio of postmax to premax fluxes. Clearly, the response of the relativistic electrons during HILDCAA events depends on the energy levels of the electrons. For $E > 0.6$ MeV electrons, significant (by a factor of >1.5) enhancements are recorded for 96% of HILDCAA events. Fully 100% of the events exhibit significant flux enhancements for $E > 2.0$ MeV electrons. Flux enhancements are significant for 48% of events for $E > 4.0$ MeV electrons.

3.3. Maximum Energy-level Dependence

Figure 4 shows the superposed variations of integrated fluxes of magnetospheric relativistic electrons for the three energy levels: $E > 0.6$, > 2.0, and > 4.0 MeV for all 35 HILDCAA events under study. The HILDCAA initiation time is taken as the zero epoch time ($t = 0$) of the superposed epoch analyses. The bold curves show the superposed mean values, and gray error bars show the standard (1σ) deviations. The HILDCAA interval is found to be characterized by enhanced fluxes, and the flux enhancement is time delayed from the HILDCAA initiation

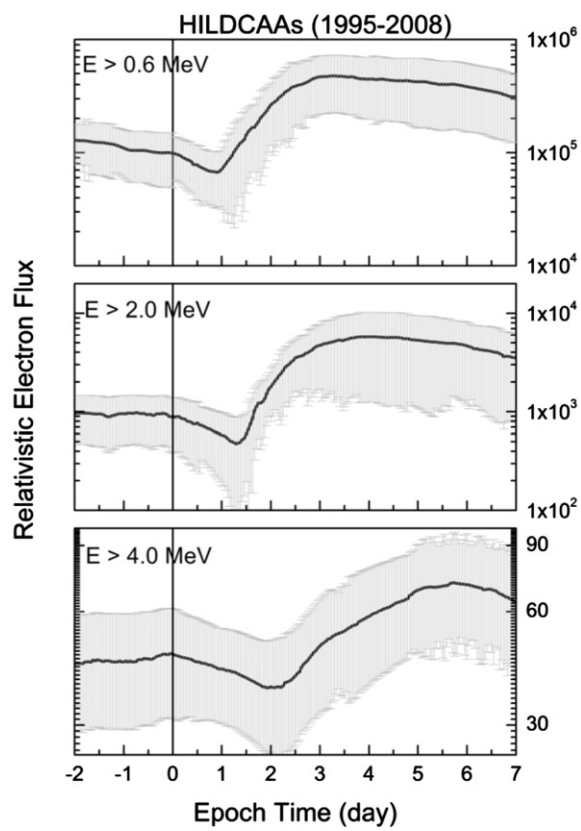

Figure 4. Superposed time series of relativistic electron fluxes (cm^{-2} s^{-1} sr^{-1}) from *GOES*. The energy levels of the electrons are given in each panel. Bold curves show the mean values, and the error bars show the standard (1σ) deviations. The zero-epoch time (indicated by the vertical line) corresponds to the initiation of HILDCAAs.

time ($t = 0$). The enhancement of $E > 0.6$ MeV electrons first starts ~1.0 day after the statistical onset of HILDCAAs. The enhancements of $E > 2.0$ and > 4.0 MeV electrons occur ~1.5 days and ~2.5 days after HILDCAA onset, respectively. Clearly, higher energy electrons take longer to respond to the HILDCAA events. After the start of flux enhancement, $E > 0.6$ MeV electrons take ~2.3 days to reach the maximum level of 4.8×10^5 FU, $E > 2.0$ MeV electrons take ~2.4 days to reach the maximum level of 5.8×10^3 FU, and $E > 4.0$ MeV electrons reach the maximum flux level of $\sim 7.2 \times 10^1$ FU after ~3.3 days. These results imply that longer acceleration timescales are needed for the higher energy electrons to be accelerated. The acceleration rates are $\sim 1.8 \times 10^5$, 2.2×10^3, and 1.0×10^1 FU d^{-1} for $E > 0.6$, > 2.0, and > 4.0 MeV electrons, respectively.

After reaching the peak levels, the fluxes decay at the rates of $\sim 0.5 \times 10^5$, 0.9×10^3, and 0.6×10^1 FU d^{-1} for $E > 0.6$, > 2.0, and > 4.0 MeV, respectively. Clearly, the decay rates are slower than the acceleration rates. From these, we estimated the probable average decay timescales of ~7.7, 5.5, and 4.0 days for $E > 0.6$, > 2.0, and > 4.0 MeV electrons, respectively. The decay timescale is the time taken to reach the pre-event flux level from the peak flux. It may be mentioned that the measurements of superposed decay rates and decay timescales may be contaminated owing to varying lengths of different HILDCAAs.

3.4. Dependence on HILDCAA Temporal Length

To study the maximum energy-level dependence on the HILDCAA temporal length, we separated HILDCAAs according to their time durations (D). The duration of the HILDCAAs under study varies between ~2 and 5 days, with an average duration of ~2.9 days for all 35 events. We separated them into two groups, one with $D \leqslant 3$ days and the other with $D > 3$ days. Twenty-four events were found to have $D \leqslant 3$ days, and 11 had $D > 3$ days. We call these events short-duration HILDCAAs and longer-duration HILDCAAs, respectively.

Figure 5 shows the comparison of electron flux enhancements for short-duration ($D \leqslant 3$ days, black curves) and longer-duration ($D > 3$ days, gray curves) HILDCAA events. As expected from the previous section, $E > 4.0$ MeV electron flux enhancement (with respect to pre-event fluxes) for short-duration events is small (~27%) compared to that for long-duration events (~82%). Flux enhancements are always larger for longer-duration events at other energy levels as well. At $E > 0.6$ MeV energy level, the flux enhancements for short- and long-duration events are ~250% and 290%, respectively. The same for $E > 2.0$ MeV electrons are ~400% and 520%, respectively. Many other differences are observed in the variations of electron fluxes between these two groups of events, which we note below.

The initial acceleration rates of the electrons are slightly lower for the longer-duration HILDCAAs compared to the short-duration ones. For the short events, the $E > 0.6$ and > 2.0 MeV electrons reach slightly higher peak fluxes compared to the longer-duration ones and start to decrease after $t \sim 3.0$ and 4.0 days, respectively. The decay rates after the short-duration HILDCAAs have ended are $\sim 0.7 \times 10^5$ and 1.2×10^3 FU d^{-1} for $E > 0.6$ and > 2.0 MeV electrons, respectively. For longer-duration HILDCAAs, the $E > 0.6$ and > 2.0 MeV fluxes appear to saturate around flux values of $\sim 4.5 \times 10^5$ and 5.6×10^3 FU, respectively. For these events, $E > 4.0$ MeV electron fluxes reach peak values ($\sim 8.3 \times 10^1$ FU) around $t \sim 5.5$ days.

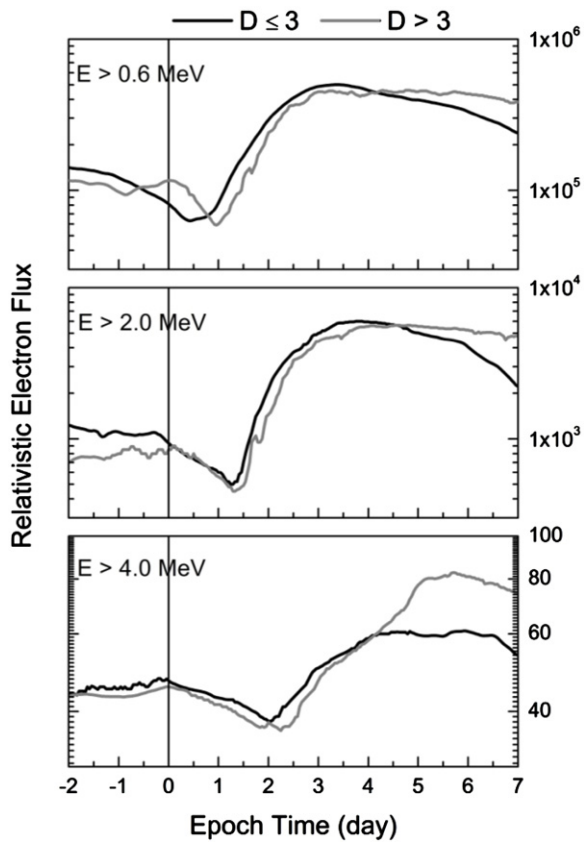

Figure 5. Panels are the same as in Figure 4: black and gray curves are for HILDCAAs with durations $D \leqslant 3$ days and $D > 3$ days, respectively. Only superposed averages are shown for clarity.

3.5. Interplanetary and Geomagnetic Conditions

Figure 6 shows that HILDCAA events order the solar wind/interplanetary and geomagnetic parameters very well. HILDCAA initiation ($t = 0$) coincides with the interface between the HSS and the slow stream in the antisolar direction (upstream) of the HSS. The region is characterized by compressions in plasma (Nsw) and IMF magnitude (Bo) and enhanced IMF Bz variance. The $t = 0$ time clearly defines the sharp southward turning of the IMF Bz and the enhancement of the interplanetary dawn-to-dusk electric field, Esw.

Several important differences in the interplanetary parameters between the two groups of events (short- and longer-duration events) may be noted in Figure 6. Although the peaks in Vsw are more or less the same (~620 km s^{-1} and 655 km s^{-1}, respectively) for short-duration and longer-duration HILDCAA events, the latter events are associated with longer-duration HSSs (as expected). After initiation of HILDCAAs, the IMF Bo is more enhanced for the $D > 3$ events than for the $D \leqslant 3$ events. After $t \sim 1.5$ days, Bz has stronger southward components, and Esw is more enhanced for longer-duration events than for short-duration ones. These lead to significant differences between these two groups of events being revealed in the polar cap index (PCI) and AE index after $t \sim 2.0$ days. Although PCI and AE values gradually decrease for short-duration events, both parameters maintain enhanced levels for longer-duration events. The PCI values are closely related with a dayside reconnection rate by the IMF southward components, and the AE indicates auroral-region substorm activity. For the longer-duration events, enhanced reconnection rates (PCI, IMF Bz) and

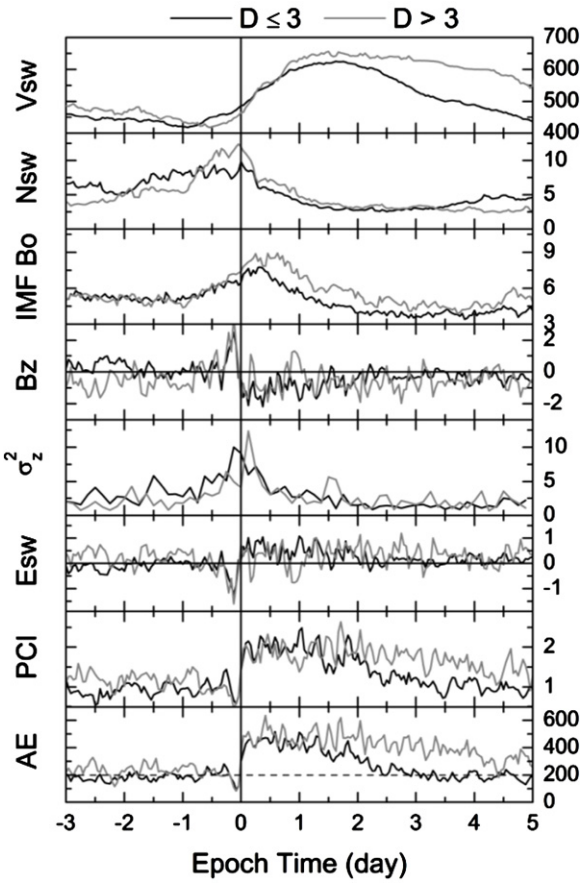

Figure 6. Superposed time series of solar wind and geomagnetic parameters from the OMNI database for HILDCAA events. From top to bottom, the panels are the solar wind speed (Vsw in km s^{-1}), the density (Nsw in cm^{-3}), IMF strength (Bo in nT), the north–southward component of the IMF (Bz in nT), the 3 hr variance of Bz (σ_z^2 in nT^2), the interplanetary dawn-to-dusk electric field (Esw in mV m^{-1}), the polar cap index (PCI), and the AE index (nT). The black and gray lines correspond to HILDCAAs with durations $D \leqslant 3$ days and $D > 3$ days, respectively, as in Figure 5. The horizontal dashed line in the AE panel indicates the AE = 200 nT level.

auroral activities (AE) after t = 2.0 days lead to the continuing injection of energetic ∼10–100 keV electrons. This is consistent with the high flux values or the saturation-like effects observed for $E > 0.6$ and > 2.0 MeV electrons and flux increases of $E > 4.0$ MeV electrons for longer-duration events (Figure 5). On the other hand, for short-duration events, Vsw drops sharply and IMF Bz is less negative after $t = 2.0$ days, leading to decreases in the PCI and AE indices. Consequently, the $E > 0.6$ and > 2.0 MeV electron fluxes start decreasing after $t \sim 3.0$ days, and no significant enhancement is recorded in $E > 4.0$ MeV electrons for short-duration events (Figure 5).

4. DISCUSSION AND CONCLUSIONS

This study reports variations of outer zone $E > 0.6$, > 2.0, and > 4.0 MeV electrons at geosynchronous orbit during HILDCAA intervals for solar cycle 23 (1995–2008). All of the 35 HILDCAA events under study were found to be characterized by flux enhancements of magnetospheric relativistic electrons of all three energies compared to the pre-event flux levels. For the $E > 2.0$ MeV electron fluxes, enhancement of >50% occurred during 100% of HILDCAAs. This result corroborates the results of Meredith et al. (2002, 2003). Relativistic electron flux enhancements were reported in the outer radiation belt during the period of prolonged substorm (AE) activity preceded by or in the absence of a geomagnetic storm main phase. Here we have used an even stricter requirement of geomagnetic activity than was assumed by Meredith et al. (2002, 2003). According to present study, the relativistic electron flux enhancements during HILDCAA intervals exhibit time lags of ∼1.0 day, ∼1.5 days, and ∼2.5 days from the statistical onset of HILDCAAs for the three energy levels, respectively. These time lags are consistent with the ∼1–2 day delays between similar features in keV- and MeV-energy electron fluxes as reported by Turner & Li (2008). The estimated average acceleration timescales for the three energy levels are ∼2.3, 2.4, and 3.3 days, respectively. Another important result is that the peak fluxes during HILDCAA events are not correlated with those before HILDCAA initiations. This implies that the fluxes in the radiation belts are not simply "pumped up" during HILDCAA events. A similar conclusion was drawn for geomagnetic storms by Reeves et al. (2003).

There are two candidate mechanisms for the relativistic electron acceleration in the magnetosphere. The first is inward radial diffusion of electrons by enhanced ULF waves (Schulz & Lanzerotti 1974; Hudson et al. 2000). In this process, electrons diffuse inward, conserving their first and second adiabatic invariants, and undergo significant energization through the betatron acceleration process. The second mechanism is local electron acceleration through resonant diffusion by whistler-mode VLF waves (Horne & Thorne 1998; Summers et al. 1998; Roth et al. 1999; Meredith et al. 2003; Thorne et al. 2013). This wave–particle interaction breaks the particle's first adiabatic invariant. It is probable that electron acceleration is due to a combination of both processes. However, it should be noted that recent observations as well as theoretical studies (Selesnick & Blake 2000; Meredith et al. 2002; Summers et al. 2002; Horne et al. 2003; Miyoshi et al. 2003; Thorne et al. 2013; Boyd et al. 2014) strongly suggest that local acceleration of electrons through a (plasma) wave–particle interaction is the dominant mechanism. Our present study supports this hypothesis. It is found that intense chorus waves exist between $L = 5$ and 10 (generally outside the plasmasphere) and at both MLT = 0–6 and 6–12 regions 100% of the time during HILDCAAs when there were simultaneous chorus observations available.

The acceleration timescales derived in this paper are consistent with theoretical timescales of electron flux enhancement by whistler-mode chorus wave acceleration (e.g., Horne et al. 2003). The delayed enhancement of higher energy electrons is a characteristic feature of wave acceleration. We propose that the relativistic electrons are bootstrapped from high-energy electrons: the $E > 0.6$ MeV electrons are accelerated by chorus from HILDCAA-injected $E \sim 10$–100 keV electrons, the $E > 2.0$ MeV electrons are accelerated from the $E > 0.6$ MeV electron population, and consequently the $E > 4.0$ MeV electrons are accelerated from the $E > 2.0$ MeV population. At this time it is uncertain how far this process will continue as the diffusion rate (by whistler-mode chorus) decreases with increasing energy. Analyses of high-energy electrons during particularly long-duration HILDCAA events are needed to answer this question from an experimental point of view.

For all of the HILDCAA events superposed, the estimated decay timescales were ∼7.7, 5.5, and 4.0 days for $E > 0.6$, > 2.0, and > 4.0 MeV electrons, respectively. For 2–6 MeV SAMPEX electrons, ∼4.6 and ⩾3.5 days loss timescales were reported by Baker et al. (2004) and Goldstein et al. (2005), respectively. Meredith et al. (2006) estimated loss timescales

of 5.5–6.5 days for ∼1 MeV electrons observed by CRRES. Our estimations of decay rates at geosynchronous orbit for $E \geqslant 0.6$ MeV electrons are consistent with these reported values.

A number of mechanisms have been proposed for the loss of the relativistic electrons: (1) cyclotron resonant interactions with electromagnetic ion cyclotron (EMIC) waves (Thorne & Kennel 1971; Summers et al. 1998; Meredith et al. 2006), (2) diamagnetic influence of the partial ring current (Ukhorskiy et al. 2006), and (3) resonant interaction with chorus leading to pitch angle scattering and loss to the atmosphere as "microbursts" (Abel & Thorne 1998; Nakamura et al. 2000; Lorentzen et al. 2001; Horne & Thorne 2003; Summers et al. 2005; Thorne et al. 2005; Tsurutani et al. 2013). Summers et al. (2007) studied the relative importance of resonant pitch angle scattering by chorus, hiss, and EMIC waves for precipitation loss of the radiation belt electrons. While loss timescales of MeV electrons due to chorus and hiss range from one day to a few days, EMIC waves can lead to even faster loss rates. As suggested by the numerical results (Albert 2003; Meredith et al. 2006; Summers et al. 2007), EMIC waves play an important role for >1 MeV electron losses, particularly at higher L values ($L \geqslant 5$). Thus, we can expect that at geosynchronous orbit (our study), EMIC waves do not scatter electrons of energy >0.6 MeV, but effectively scatter the more energetic (>2.0 and >4.0 MeV) electron population. This is consistent with the shorter loss timescales of $E > 2.0$ and > 4.0 MeV electrons compared to the $E > 0.6$ MeV electrons observed in the present study.

Another important result of the present study is the maximum energy-level dependence on the HILDCAA duration. The intense substorm/convection events that comprise the high-intensity, long-duration, and continuous AE intervals of the HILDCAAs are responsible for frequent and intense injections of anisotropic ∼10–100 keV electrons into the magnetosphere. These electrons are a source for the generation of chorus and the acceleration to even higher MeV energies. When short-duration ($D \leqslant 3$ days) events end after ∼3.0 days, the relativistic electrons undergo different loss processes and the fluxes decay gradually. On the other hand, for longer-duration ($D > 3$ days) events, ∼10–100 keV electrons are sporadically but continuously injected into the magnetosphere. These electrons are accelerated to >0.6 MeV and consequently to higher ($E > 2.0$ and > 4.0 MeV) energies, as proposed above. Different loss processes may occur simultaneously with the acceleration. The possible saturation-like effect observed in $E > 0.6$ MeV and $E > 2.0$ MeV electrons for longer-duration HILDCAAs may be due to a balance between acceleration and loss processes.

5. FINAL COMMENTS

The strong relationship between relativistic electrons and HILDCAAs shown in this paper indicates that the scenario discussed at the beginning of the paper seems to be valid. The occurrence of HILDCAAs indicates that ∼10–100 keV electrons are being injected into the magnetosphere, chorus is being generated by these anisotropic electrons, and chorus is interacting with the ∼100 keV portion of this electron distribution to accelerate the particles to even higher energies. Thus, HILDCAAs may therefore be a good proxy for continuous chorus generation in the $00 < \mathrm{MLT} < 12$ sector whenever spacecraft measurements of the waves are not possible.

This paper indicates that the longer the HILDCAAs (and chorus) last, the higher the energy of relativistic electrons will be (Thorne et al. 2013). An interesting question is, will there be a level where saturation takes place, and if so, at what energies? The way to better understand the limits to this acceleration process is to make observations during extremely long-duration HILDCAA intervals. Some events with ∼12 to 25 day durations were noted in the 1973–1975 time frame (Tsurutani et al. 1995). Such unusual events have not happened again. It would be interesting to reexamine such older data or, better yet, see if events of this type occur during the modern Van Allen Probe epoch, to give high priority to study those events.

As a final comment, we mention that the hypothesis of slow stirring of the solar photosphere, creating $T \sim 15$ minutes to ∼2 hr period Alfvén waves that are carried by the solar wind to a distance 1.5×10^8 km (1 AU) away to create approximately MeV electrons, seems a bit preposterous. If it were not for the diligence and hard work of the space plasma community, this long string of physical processes would never have been uncovered.

The work of R.H. is financially supported by Fundação de Amparo à Pesquisa do Estado de São Paulo (FAPESP) through a postdoctoral research fellowship at INPE. E.E. would like to thank the Brazilian CNPq (301233/2011-0) agency for financial support. Portions of this research were performed at the Jet Propulsion Laboratory, California Institute of Technology, under contract with NASA. O.S. acknowledges funding from grants GACR205-10/2279 and LH14010. The Cluster data can be obtained from ESA CFA. The *GOES* data used in this paper are collected from the website http://www.ngdc.noaa.gov/stp/satellite/goes/dataaccess.html. The OMNI data are collected from http://omniweb.gsfc.nasa.gov/.

REFERENCES

Abel, B., & Thorne, R. M. 1998, JGRA, 103, 2385
Albert, J. M. 2003, JGRA, 108, 1249
Baker, D. N., Blake, J. B., Klebesadel, R. W., & Higbie, P. R. 1986, JGRA, 91, 4265
Baker, D. N., Kanekal, S. G., Li, X., et al. 2004, Natur, 432, 878
Baker, D. N., Kanekal, S. G., Pulkkinen, T. I., & Blake, J. B. 1999, GeoRL, 26, 3193
Belcher, J. W., & Davis, L., Jr. 1971, JGRA, 76, 3534
Boyd, A. J., Spence, H. E., Claudepierre, S. G., et al. 2014, GeoRL, 41, 2275
Brice, N., & Lucas, C. 1971, JGRA, 76, 900
DeForest, S. E., & McIlwain, C. E. 1971, JGRA, 76, 3587
Dungey, J. W. 1961, PhRvL, 6, 47
Goldstein, J., Kanekal, S. G., Baker, D. N., & Sandel, B. R. 2005, GeoRL, 32, L15104
Gonzalez, W. D., Guarnieri, F. L., Clua-Gonzalez, A. L., et al. 2006, in Recurrent Magnetic Storms: Corotating Solar Wind Streams, ed. B. T. Tsurutani et al. (Washington, DC: AGU), 175
Gonzalez, W. D., Joselyn, J. A., Kamide, Y., et al. 1994, JGRA, 99, 5771
Gonzalez, W. D., & Mozer, F. S. 1974, JGRA, 79, 4186
Guarnieri, F. L. 2006, in Recurrent Magnetic Storms: Corotating Solar Wind Streams, ed. B. T. Tsurutani et al. (Washington, DC: AGU), 235
Hajra, R., Echer, E., Tsurutani, B. T., & Gonzalez, W. D. 2013, JGRA, 118, 5626
Hajra, R., Echer, E., Tsurutani, B. T., & Gonzalez, W. D. 2014a, JGRA, 119, 2675
Hajra, R., Echer, E., Tsurutani, B. T., & Gonzalez, W. D. 2014b, JASTP, 121, 24
Hajra, R., Tsurutani, B. T., Echer, E., & Gonzalez, W. D. 2014c, GeoRL, 41, 1876
Horne, R. B. 2003, Proceedings of ESA Workshop (Noordwijk, The Netherlands: ESTEC)
Horne, R. B., Glauert, S. A., & Thorne, R. M. 2003, GeoRL, 30, 1493
Horne, R. B., & Thorne, R. M. 1998, GeoRL, 25, 3011
Horne, R. B., & Thorne, R. M. 2003, GeoRL, 30, 1527
Hudson, M. K., Elkington, S. R., Lyon, J. G., & Goodrich, C. C. 2000, AdSpR, 25, 2327
Inan, U. S., Bell, T. F., & Helliwell, R. A. 1978, JGRA, 83, 3235
Jentsch, V. 1976, JGRA, 81, 135

Kennel, C. F., & Petschek, H. E. 1966, JGRA, 71, 1
Kozyra, J. U., Crowley, G., Emery, B. A., et al. 2006, in Recurrent Magnetic Storms: Corotating Solar Wind Streams, ed. B. T. Tsurutani et al. (Washington, DC: AGU), 319
Lorentzen, K. R., Blake, J. B., Inan, U. S., & Bortnik, J. 2001, JGRA, 106, 6017
Meredith, N. P., Cain, M., Horne, R. B., et al. 2003, JGRA, 108, 1248
Meredith, N. P., Horne, R. B., & Anderson, R. R. 2001, JGRA, 106, 13165
Meredith, N. P., Horne, R. B., Glauert, S. A., et al. 2006, JGRA, 111, A05212
Meredith, N. P., Horne, R. B., Iles, R. H. A., et al. 2002, JGRA, 107, 1144
Meredith, N. P., Horne, R. B., Sicard-Piet, A., et al. 2012, JGRA, 117, A10225
Miyoshi, Y., Morioka, A., Obara, T., et al. 2003, JGRA, 108, 1004
Nakamura, R., Isowa, M., Kamide, Y., et al. 2000, JGRA, 105, 15875
Onsager, T. G., Grubb, R., Kunches, J., et al. 1996, Proc. SPIE, 2812, 281
Paulikas, G. A., & Blake, J. B. 1979, in Quantitative Modeling of Magnetospheric Processes, ed. W. Olsen (Washington, DC: AGU), 180
Reeves, G. D., McAdams, K. L., Friedel, R. H. W., & O'Brien, T. P. 2003, GeoRL, 30, 1529
Reeves, G. D., Spence, H. E., Henderson, M. G., et al. 2013, Sci, 341, 991
Roth, I., Temerin, M. A., & Hudson, M. K. 1999, AnGeo, 17, 631
Santolik, O., Gurnett, D. A., Pickett, J. S., Chum, J., & Cornilleau-Wehrlin, N. 2009, JGRA, 114, A00F03
Santolik, O., Macusova, E., Kolmasova, I., Cornilleau-Wehrlin, N., & de Conchy, Y. 2014, GeoRL, 41, 2729
Santolik, O., Pickett, J. S., Gurnett, D. A., et al. 2010, JGRA, 115, A00F13
Schulz, M., & Lanzerotti, L. 1974, Particle Diffusion in the Radiation Belts (New York: Springer)
Selesnick, R. S., & Blake, J. B. 2000, JGRA, 105, 2607
Smith, E. J., Tsurutani, B. T., & Rosenberg, R. L. 1978, JGRA, 83, 717
Summers, D., Ma, C., Meredith, N. P., et al. 2002, GeoRL, 29, 2174
Summers, D, Mace, R. L., & Hellberg, M. A. 2005, JPlPh, 71, 237
Summers, D., Ni, B., & Meredith, N. P. 2007, JGRA, 112, A04207
Summers, D., Thorne, R. M., & Xiao, F. 1998, JGRA, 103, 20487
Thorne, R. M., & Kennel, C. F. 1971, JGRA, 76, 4446
Thorne, R. M., Li, W., Ni, B., et al. 2013, Natur, 504, 411
Thorne, R. M., O'Brien, T. P., Shprits, Y. Y., Summers, D., & Horne, R. B. 2005, JGRA, 110, A09202
Tsurutani, B. T., & Gonzalez, W. D. 1987, P&SS, 35, 405
Tsurutani, B. T., Gonzalez, W. D., Gonzalez, A. L. C., et al. 1995, JGRA, 110, 21717
Tsurutani, B. T., Ho, C. M., Smith, E. J., et al. 1994, GeoRL, 21, 2267
Tsurutani, B. T., Horne, R. B., Pickett, J. S., et al. 2010, JGRA, 115, A00F01
Tsurutani, B. T., & Lakhina, G. S. 1997, RvGeo, 35, 491
Tsurutani, B. T., Lakhina, G. S., & Verkhoglyadova, O. P. 2013, JGRA, 118, 2296
Tsurutani, B. T., McPherron, R. L., Gonzalez, W. D., et al. 2006, in Recurrent Magnetic Storms: Corotating Solar Wind Streams, ed. B. T. Tsurutani et al. (Washington, DC: AGU), 1
Tsurutani, B. T., & Smith, E. J. 1974, JGRA, 79, 118
Tsurutani, B. T., & Smith, E. J. 1977, JGRA, 82, 5112
Tsurutani, B. T., Smith, E. J., West, H. I., & Buck, R. M. 1979, in Waves Instabilities in Space Plasmas, ed. P. J. Palmadesso & K. Papadopoulos (Norwell, MA: Reidel), 55
Turner, D. L., & Li, X. 2008, SpWea, 6, S05005
Turner, N. E., Mitchell, E. J., Knipp, D. J., & Emery, B. A. 2006, in Recurrent Magnetic Storms: Corotating Solar Wind Streams, ed. B. T. Tsurutani et al. (Washington, DC: AGU), 113
Ukhorskiy, A. Y., Anderson, B. J., Brandt, P. C., & Tsyganenko, N. A. 2006, JGRA, 111, A11S03
Wrenn, G. L. 1995, JSpRo, 32, 514